EVALUATION OF CARBON-ROD REINFORCED CRIPPLING STRENGTH SPECIMENS

Donald J. Baker*
Vehicle Technology Center - ARL
NASA Langley Research Center
Hampton VA 23681
and
Carl Q. Rousseau**
Bell Helicopter, Textron, Inc.
Ft. Worth, TX 76101

Abstract

The results of an experimental and analytical investigation of the crippling strength of carbon-rod reinforced specimens are presented. One-Edge-Free and No-Edge-Free crippling specimens with width-to-thickness ratios of 6.8 to 27 and 12.6 to 45, respectively, are investigated. Empirical crippling strength design curves have been developed for carbon-rod reinforced One-Edge-Free and No-Edge-Free crippling specimens. The carbon-rod reinforced crippling strength data are compared to carbon-tape crippling strength data. The carbon-tape preliminary laminate design curves recommended by MIL-HDBK-17E provide a conservative design for the One-Edge-Free structural elements and an acceptable design for the No-Edge-Free structural elements. Results of a nonlinear finite element analysis conducted for each configuration are presented.

Introduction

The use of prefabricated pultruded carbon-epoxy rods has reduced the manufacturing complexity and cost of composite structures without decreasing structural efficiency. This concept of replacing conventional unidirectional carbon fibers with carbon-epoxy rods embedded in a syntactic adhesive minimizes fiber waviness and increases laminate stiffness and strength. The pioneering research and development work for carbon-rod reinforced composite structures was done by Bell Helicopter, NASA, and the Air Force and is outlined in references 1-9. The crippling strength of structural elements with pultruded carbon-epoxy rods has not been investigated in references 1-9. The main objective of the present study is to generate empirical relations for crippling strength curves that can be used in the design of carbon-rod crippling elements. The secondary objectives of the study are to determine if carbon-tape crippling strength curves could be used for the design of carbon-rod-reinforced elements, and to predict the geometric nonlinear behavior of the carbon-rod crippling elements.

Symbols

b	Test element width, inches.
t	Test element thickness, inches.
E_x	Longitudinal modulus of laminate, psi.
E_y	Transverse modulus of laminate, psi.
$\bar{E}$	Effective modulus, psi.
F_{cc}	Crippling strength, psi.
F_{cu}	Laminate ultimate strength, psi.
P_{cr}	Buckling load, lbs.
P_{max}	Failure load, lbs.

Specimens

Test specimens for One-Edge-Free (OEF) and No-Edge-Free (NEF) element configurations were designed by Bell Helicopter, Textron using equal-flange-thickness tape crippling strength curves, such as those found in MIL-HDBK-17E, Volume 3, Figures 4.7.2.4(a) and (b) (reference 10), despite the significant differences in the flange thicknesses. In addition to sizing the specimen width-to-thickness (b/t) ratios to yield a range of data without other global buckling or crushing failure modes, a predicted maximum failure load, P_{max}, also resulted from this design process and is included in table 1. The resulting specimen configurations are shown in figure 1a for the OEF specimens and in figure 1b for the NEF specimens. Each test specimen has two test elements and each element is a laminate of $\pm 45°$ carbon-epoxy tape (Hexcel IM7/8552, grade 190) and two layers of pultruded carbon-epoxy rods (Neptco 0.067-inch-diameter IM7 rods) embedded in a syntactic adhesive

* Aerospace Engineer, Structural Mechanics Branch
** Principal Engineer, Research Structures

Table 1. Summary of buckling and failure loads.

Specimen type[a]	b/t	Predicted buckling load, kips	Predicted number of half-waves, modes 1 and 2	Predicted failure load, kips	Experimental buckling load, kips	Failure load, kips
OEF	6.8	29.7	1	43.8	29.5	31.1
OEF	12.6	27.8	1	49.8	26.0	37.7
OEF	19.4	31.2	1	54.1	28.5	51.0
OEF	27.0	37.5	1	57.7	32.0	58.3
NEF	12.6	78.2	[c]	75.0	NB[b]	65.8
NEF	19.4	85.2	3	81.4	84.1	84.5
NEF	27.0	66.6	2	86.7	73.0	79.4
NEF	45.0	49.4	1	95.4	56.0	86.7

[a] Specimen type:
OEF – One-Edge-Free
NEF – No-Edges-Free
[b] NB - No buckling observed
[c] No buckling predicted in elements

(Hysol HC9872) which is sandwiched between the tape layers. The carbon-epoxy tape is continued between each test element of the specimen to support one edge on the OEF and both edges on the NEF specimens. The OEF specimen design shown in figure 1a is a combination of two one-edge-free specimens that are usually tested to determine the crippling strength. To clarify the results later in this paper the test elements will be identified as element 1 and 2 as shown in figure 1a. The NEF specimen also has two test elements and they will be identified as element 1 and 2 as shown in figure 1b. All specimens have the same test element thickness, and the distance between the elements is 2.0 inches. The width of the test element was varied to produce specimens with various width-to-thickness (b/t) ratios. The element b/t ratios vary from 12.6 to 45 for the NEF specimens and from 6.8 to 27 for the OEF specimens. The NEF specimens are 23-inches long and the OEF specimens are 14-inches long before potting the ends for testing. The specimens were fabricated by Bell Helicopter on multi-piece aluminum IML tools. The OML surface was bagged and the parts were autoclave-cured using the appropriate Bell process specification.

Test Procedure

All specimens were instrumented with strain gages. The layout for the strain gages on an OEF specimen with b/t = 19.6 is shown in figure 2. The gages on the other specimens had similar patterns with the number of gages varying from 12 to 36 depending on the size of the specimen. Out-of-plane displacements were measured by linear variable displacement transducers (LVDT) located as shown by the open squares in figure 2. The number of LVDT's varies with the specimen size. One surface (element 2) of each specimen was painted white to be used with a moiré interferometry technique. Out-of-plane displacements on element 1 were determined with the LVDT's.

All specimen tests were performed at room temperature in the as-fabricated condition. The specimens were placed between the platens of a hydraulic test machine and loaded in compression at a rate of 3,000 lbs./min. for the OEF specimens and a rate of 5,000 lbs./min. for the NEF specimens. A video camera and a still camera recorded the changes in the moiré fringe pattern during the tests. The load, strain, out-of-plane and head displacements were recorded with a computer-controlled data acquisition system for each test.

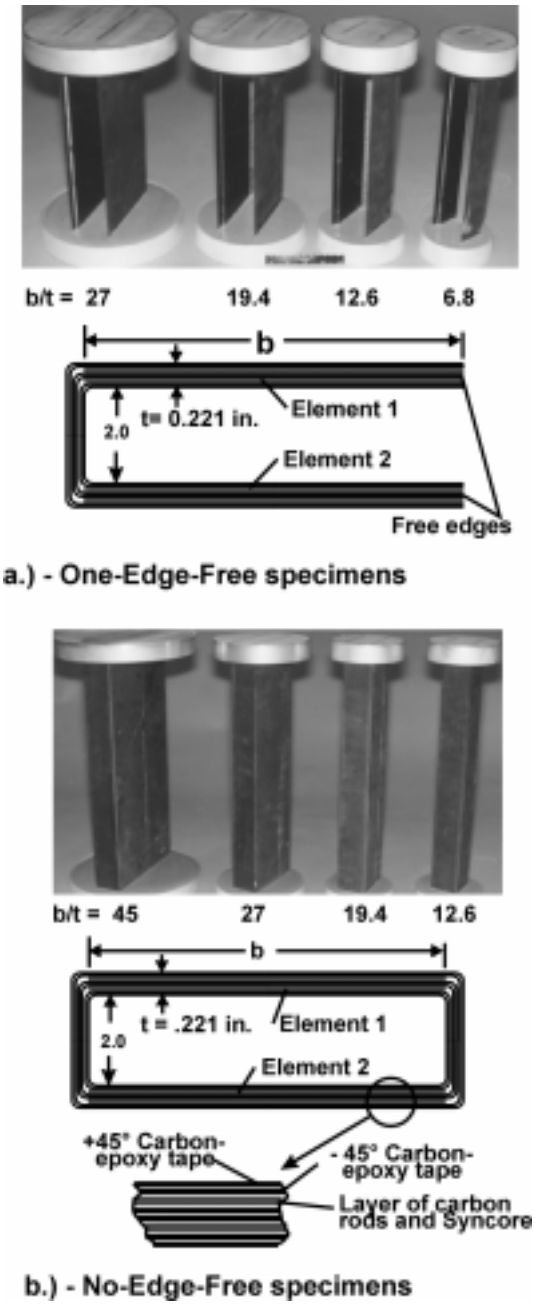

Figure 1. - Crippling test specimens.

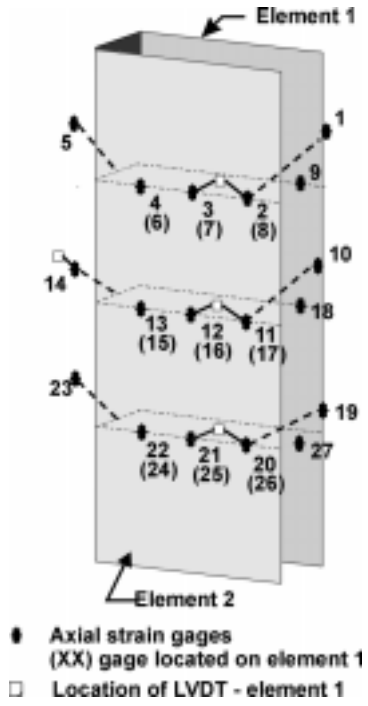

Figure 2. - Location of instrumentation used on OEF specimen, b/t =19.6.

Analysis

A finite element analysis was conducted for each design configuration (i.e., each test element b/t ratio) using the STAGS nonlinear structural analysis code (reference 11) to determine the initial linear buckling load and geometrically nonlinear responses. STAGS is a finite element code for the general-purpose analysis of shell structures of arbitrary shape and complexity. A 9-node quadrilateral shell element, STAGS element 480, was used in the analysis. The number of elements for each specimen was varied according to specimen size to give approximately the same size element for all of the analyses. A finite element model for an OEF specimen with b/t = 19.4 is shown in figure 3. The group of elements that represent elements 1 and 2 in the test specimens are also identified as elements 1 and 2 in figure 3. The predicted first four buckling mode shapes and critical loads for the OEF specimen are shown in figure 4. The elements 1 and 2 buckle into a single half-wave for the first two modes, with elements 1 and 2 deflecting in opposite directions for the first mode and the elements deflect in the same direction for the second mode. Only 26 pounds separate the critical loads for the first and second modes. The elements buckle into two half-waves for third and fourth modes. The elements deflect in the same direction for the third mode while the elements deflect in opposite directions for fourth mode. The predicted mode shapes for all OEF specimens was a single half-wave for the first two modes and two half-waves for the third and fourth modes.

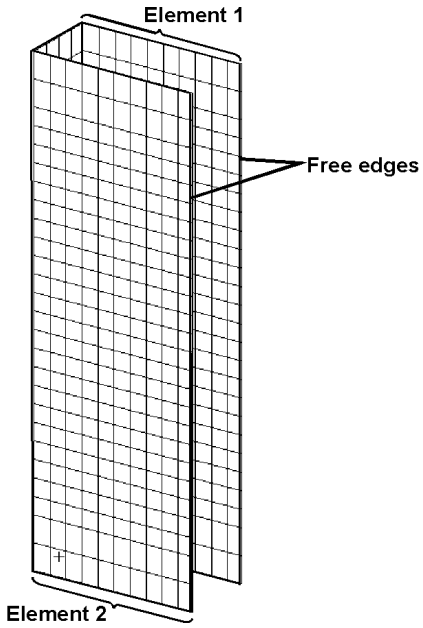

Figure 3. - Finite element model of OEF specimen, b/t = 19.6.

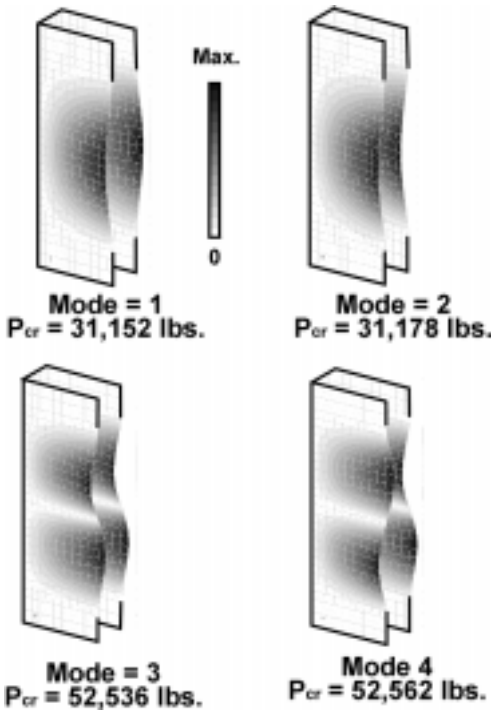

Figure 4. - Predicted mode shapes and critical loads for OEF specimen, b/t = 19.6.

A finite element model for a NEF specimen with a b/t = 45 is shown figure 5. The predicted first four buckling mode shapes and critical loads for the NEF specimen are shown in figure 6. Only one-half of the specimen width is shown in figure 6 to help illustrate the mode shapes. Elements 1 and 2 buckle into a single half-wave for the first and second modes and into two half-waves for the third and fourth modes, with the only difference between the first and second modes or the third or fourth modes is in the direction of their deflection. The analysis of the NEF specimen with b/t = 12.6 predicted only local buckling in the shorter ±45° web between elements 1 and 2, near the potted ends. The analysis of the NEF specimen with b/t = 19.4 predicted three half-waves for the first and second modes and four half-waves for the third and fourth mode. Analysis of the NEF specimen with b/t = 27 predicted two half-waves for the first and second modes and three half-waves for the third and fourth modes. A summary of the initial buckling load predictions and number of half-waves for the first and second modes for all specimens are shown in table 1. The STAGS code was also used to perform a nonlinear analysis of each specimen configuration and selected results are shown with the corresponding experimental results in subsequent figures.

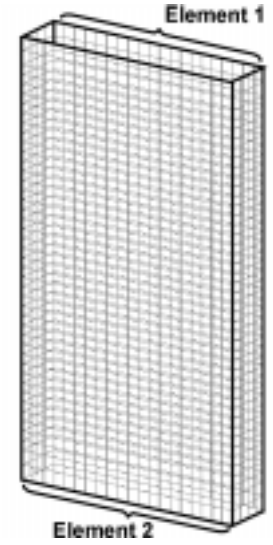

Figure 5. - Finite element model of NEF specimen, b/t = 45.

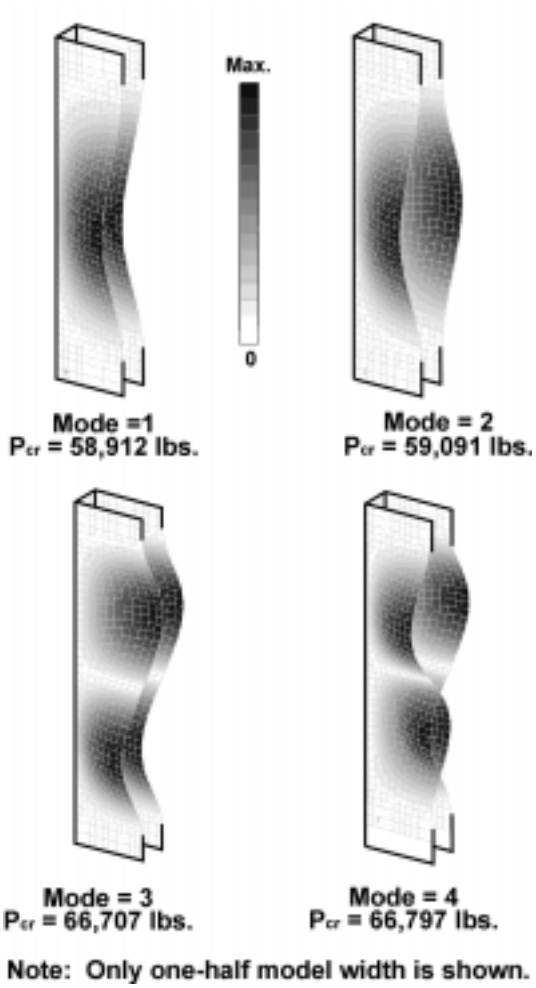

Figure 6. - Predicted mode shapes and critical loads for NEF specimen, b/t = 45.

Results and Discussion

One-Edge-Free specimens

Selected experimental results and nonlinear analysis results for OEF specimens are shown in figures 7 through 10. The experimental response and predicted analytical end-shortening response for all OEF specimens are shown in figure 7. Good agreement is shown between the predicted response from the nonlinear analysis and the experimental results. Results from back-to-back strain gages at the mid-length of the specimen, near the free edge of the elements 1 and 2 of an OEF specimen (b/t = 19.4) are shown in figure 8. The elements buckle at a load of 28.5 kips which compares well with the predicted buckling load of 31.2 kips (see table 1). The specimen continues to support load

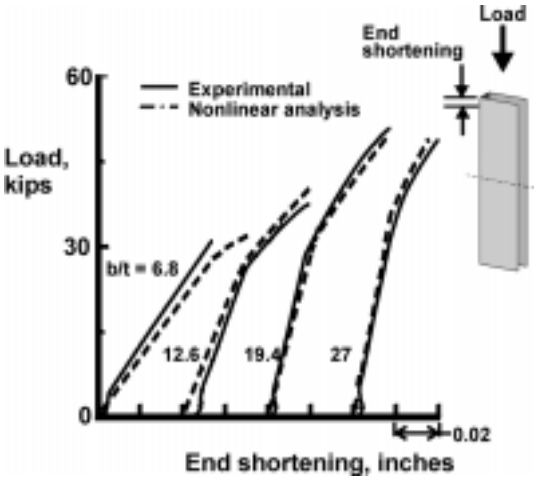

Figure 7. - Specimen end-shortening as function of the load for all OEF specimens.

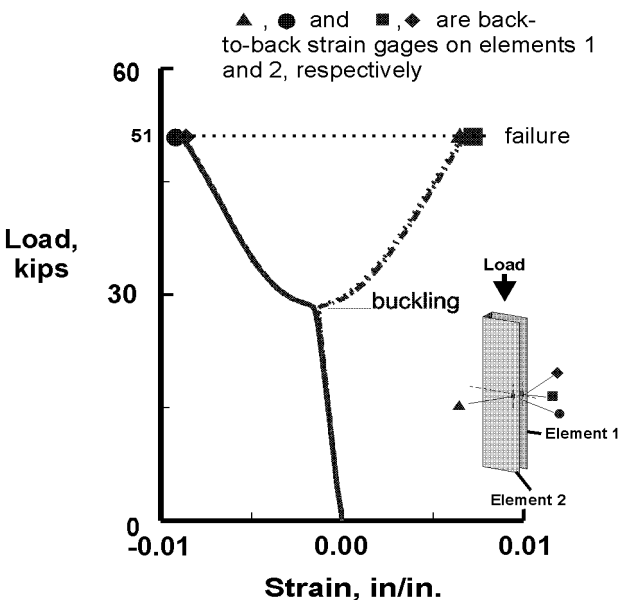

Figure 8. - OEF strain gages results on free edge, b/t = 19.6.

up to failure at 51.0 kips. Both elements show identical responses. The out-of-plane displacement at the same location as the strain gages is shown in figure 9. The predicted out-of-plane displacement is also shown in figure 9 and compares well with the experimental results. A summary of the results for all OEF specimens is given in table 1 and in the bar chart shown in figure 10. Comparison of columns 3 and column 6 in table 1 or the first two bars for each b/t ratio in figure 10 indicates that the OEF specimens buckled at

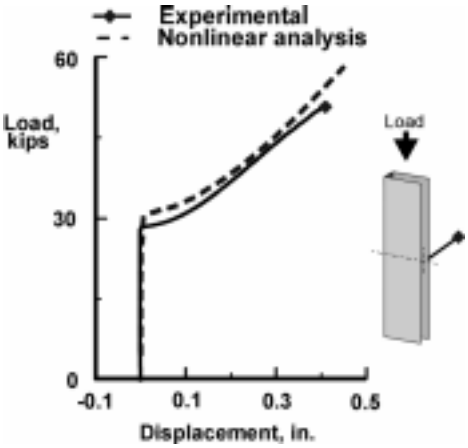

Figure 9. - Out-of-plane displacement at center of element 1.

85 percent to 99 percent of the predicted buckling loads. The OEF specimen with b/t = 6.8 failed at approximately 6 kips after observed buckling and did not exhibit any noticeable out-of-plane deflections before failure. Specimens with b/t = 12.6, 19.4, and 27 followed the same trend of buckling into a single half-wave, then supported load into the post-buckling load range. All OEF specimens indicated good comparison between the predicted displacement response and experimental results. Comparison of columns 5 and column 7 in Table 1 or the third and fourth bars for each b/t ratio in figure 10 indicates that the failure loads were 71 percent to 101 percent of the predicted failure loads.

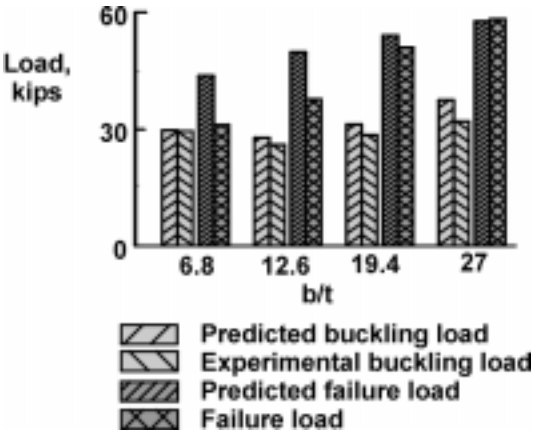

Figure 10. - Summary of buckling loads, and failure loads for OEF specimens.

The ratio of the crippling strength to the laminate ultimate strength for the OEF carbon-rod reinforced specimens are compared in figure 11 with the MIL-HDBK-17E (reference 10) recommended preliminary design curves (figure 4.7.2(h)) for the [$\pm$45/0$_n$/$\pm$45] carbon-tape laminates. The strength ratios for the OEF specimens (figure 11) are 18 percent to 50 percent above the predicted ratios from the MIL-HDBK-17E preliminary design curves. These results suggest that using the carbon-tape preliminary design curves for the design of carbon-rod reinforced structure would produce conservative designs for the OEF elements.

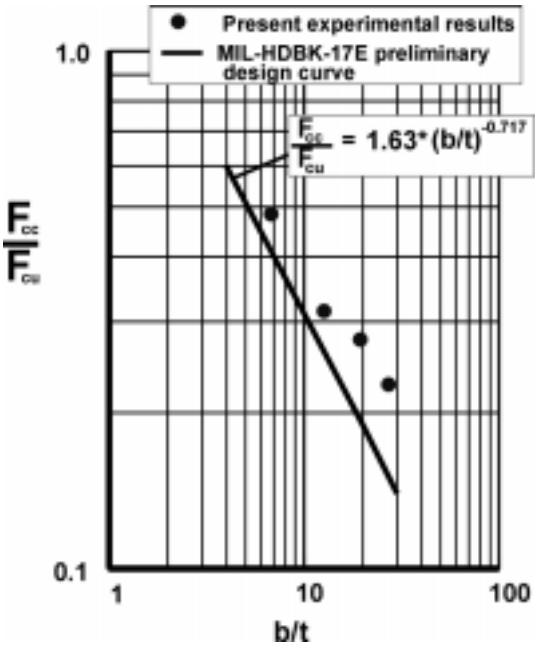

Figure 11. - Comparison of experimental data to MIL-17-HDBK preliminary design curves.

Typical failure modes for OEF specimens are shown in the figure 12. All OEF specimens delaminated along the free edge through the $\pm$45° ply between the layers of rods. The layer of rods on the compression side of the OEF specimens with b/t = 12.6 and 19.4 failed across the width of one element of each specimen. All specimens exhibited some failures in the corner radius locations where the elements transitioned to the $\pm$45° tape laminate webs that support the flanges.

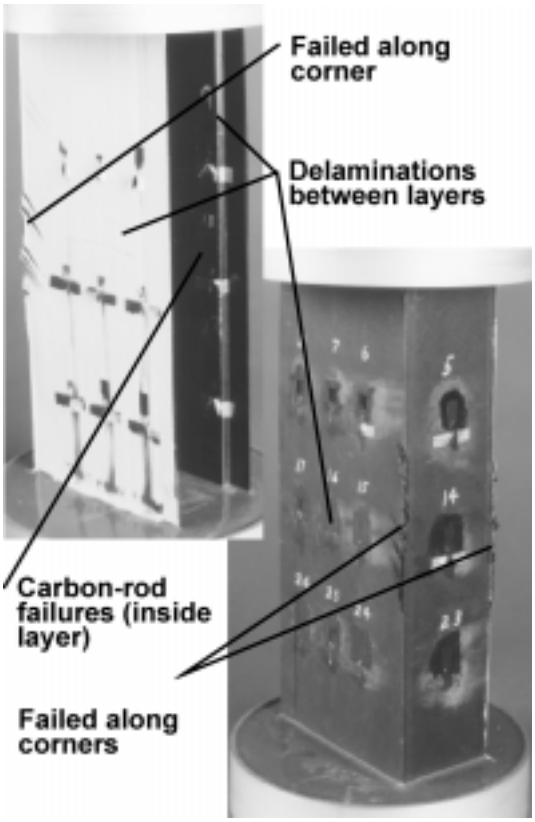

Figure 12. - Typical failure modes for OEF specimens.

The crippling strength of elements is usually determined from non-dimensional crippling strength curves. Different normalization techniques have been suggested for composite structures than those used for metallic structures. The non-dimensional parameters suggested by MIL-HDBK-17E for normalization of the data are as follows:

$$\frac{F_{cc}}{F_{cu}}\frac{E_x}{\overline{E}} \quad \text{and} \quad \frac{b}{t}\frac{\overline{E}}{E_x}\sqrt{\frac{F_{cu}}{\sqrt{E_x E_y}}}$$

where: $\overline{E} = \dfrac{12D_{11}}{t^3}\left(1-\nu_{xy}\nu_{yx}\right)$ is an effective modulus accounting for the stacking sequence. The experimental results for the OEF specimens have been normalized by the above parameters, and are shown in figure 13. A curve is fitted through the data and the values of the curve fit parameters are shown in figure 13. These curves can be used to design the OEF carbon-rod reinforced structural elements. Test results of OEF specimens of graphite-thermoset and graphite-thermoplastic tape systems normalized by the same parameters are shown in MIL-HDBK-17E, figure 4.7.2.4(a) and are also shown in figure 13 for comparison. The tape data from MIL-HDBK-17E falls above the carbon-rod data for low b/t ratios and below the carbon-rod data for high b/t ratios.

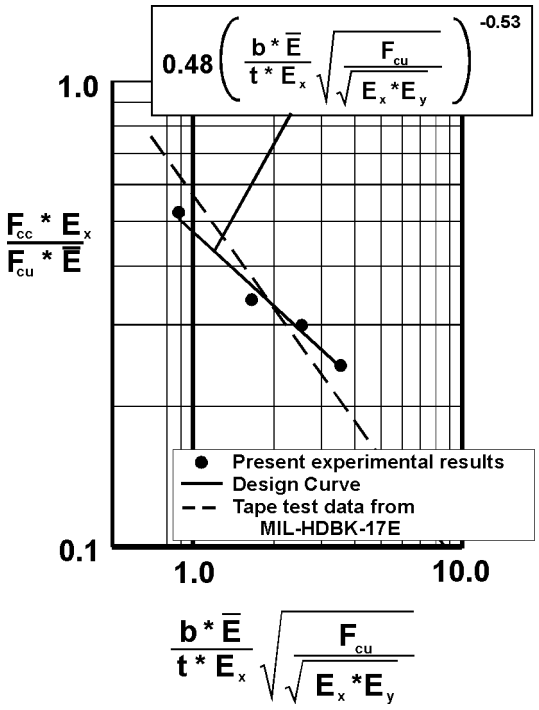

Figure 13. - Design curve for One-Edge-Free elements.

No-Edge -Free specimens

The experimental end-shortening responses for all NEF specimens are shown in figure 14. Also included in figure 14 is the predicted response from a STAGS nonlinear analysis of each configuration. Good agreement is shown between the response predicted by the nonlinear analysis and the experimental results. A summary of the results for all NEF specimens is shown in table 1 and in the bar chart shown in figure 15. Each NEF specimen will be evaluated individually in the following paragraphs.

The NEF specimen with a b/t = 12.6 failed at approximately at 88 percent of the predicted failure load (table 1) and 84 percent of the predicted buckling load. The strain gage response was linear to failure.

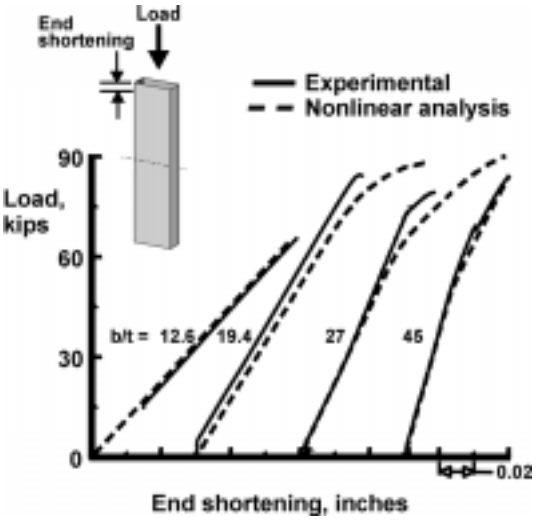

Figure 14. - Specimen end-shortening as a function of load for all NEF specimens

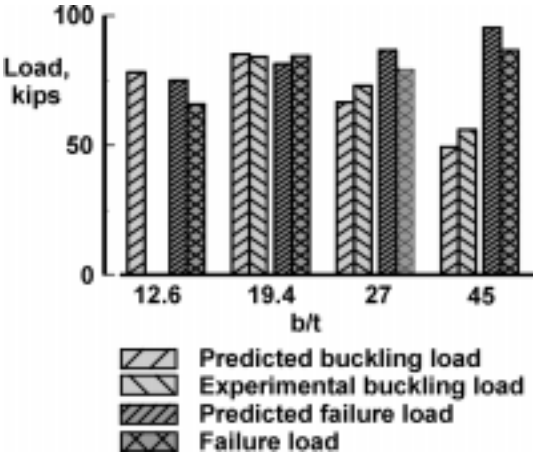

Figure 15. - Summary of buckling loads and failure loads for NEF specimens.

The NEF specimen with a b/t =19.4 buckled into three half-waves as shown by the moiré fringe pattern in figure 16a at 99 percent of the predicted buckling load. The final deformed shape as determined from the strain gages and the LVDT's is shown in figure 16b. Only half of the specimen width is shown in figure 16b to help illustrate the deformed shape. This deformed shape is similar to the predicted shape for the second mode (see figure 17) except each element deflects in the opposite direction from the predicted direction. The failure load is 104 percent of the predicted failure load (figure 15).

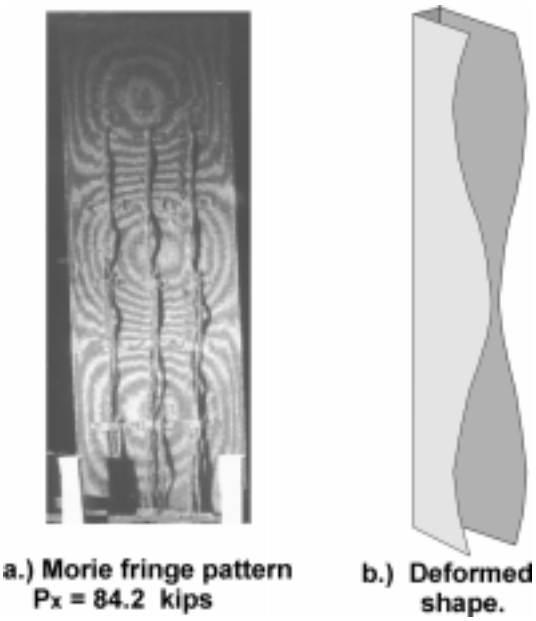

Figure 16. - Deformed shape of NEF specimen with b/t = 19.4.

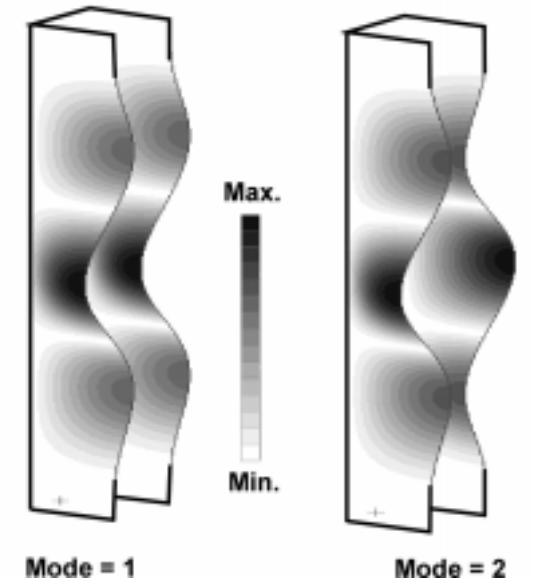

Figure 17. - Predicted mode shape for NEF specimen with b/t = 19.4.

The NEF specimen with b/t = 27 buckled at 73.2 kips which is 110 percent of the predicted buckling load (see figure 15). The specimen buckled into two half-waves as shown by the moiré fringe pattern in figure 18a. The final deformed shape as determined from the

strain gages and the LVDT's is shown in figure 18b. This deformed shape compares well with the predicted shape for the first mode shown in figure 19. The out-of-plane displacement response is shown in figure 20 for three locations on element 1. As shown in figure 20, very little out-of-plane deflection is indicated until the bifurcation point where the top and bottom locations (filled triangle and filled circle) deflect in opposite directions and the mid-length location shows very little deflection. The predicted out-of-plane response is also shown in figure 20 for the same three points. The failure load (figure 15) is 92 percent of the predicted failure load

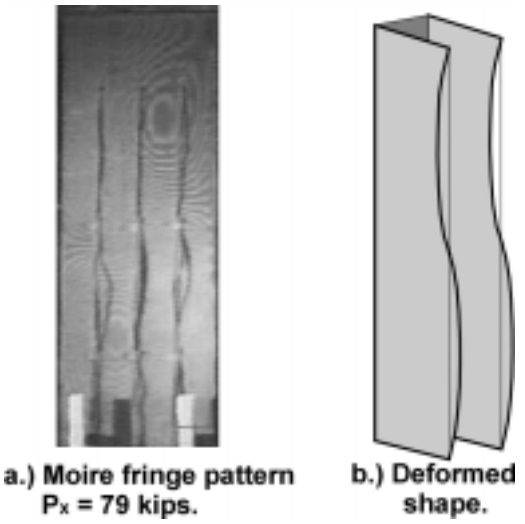

Figure 18. - Deformed shape for NEF specimen with b/t = 27.

The NEF specimen with b/t = 45 buckled into a single half-wave at 56 kips which is 113 percent of the predicted buckling load (figure 15). A small load relaxation in the end-shortening curve (figure 14) at approximately 70 kips of load for the NEF specimen with b/t = 45 results from a mode change in one element as can be observed in the following figures. The change in mode shape from a single half-wave to two half-waves is shown in figure 21b and the strain reversal in the axial strain gages on element 1 occurs at approximately 70 kips of load level. The strain gages on element 2 of the specimen are shown in figure 21a and do not indicate a mode change, but do indicate a small perturbation in the strain at the 70 kip load. The mode change is also shown in figure 22, where the out-of-plane displacement noted by the filled circle and filled square change from a positive displacement to a negative displacement, and the displacement noted by the filled triangle increases in the positive direction. The video recording of the moiré fringe pattern did not indicate a change in the mode of element 2. The predicted displacements from a STAGS nonlinear analysis are also shown in figure 22 and they compare well with the experimental results up to the mode change.

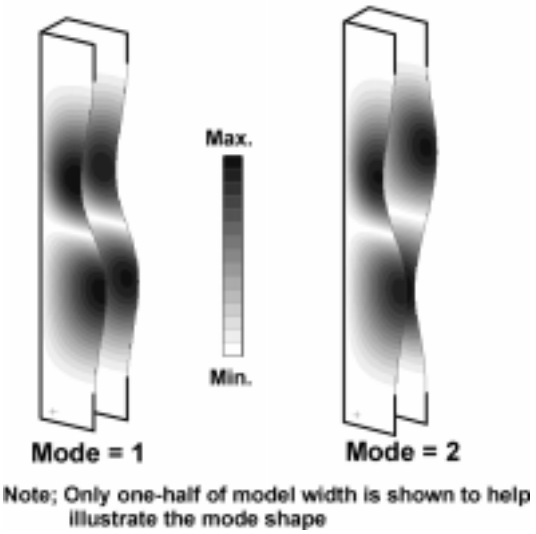

Figure 19. - Predicted mode shape for NEF specimen with b/t = 27.

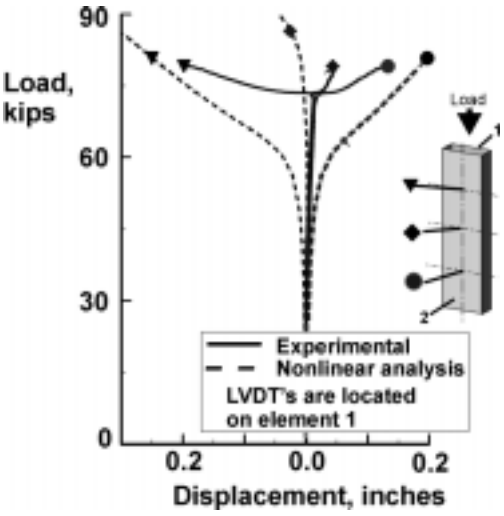

Figure 20. - Out-of-plane displacement for NEF specimen with b/t = 27.

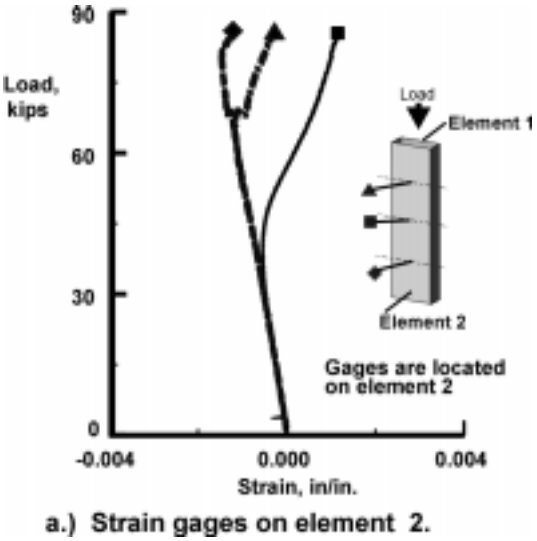

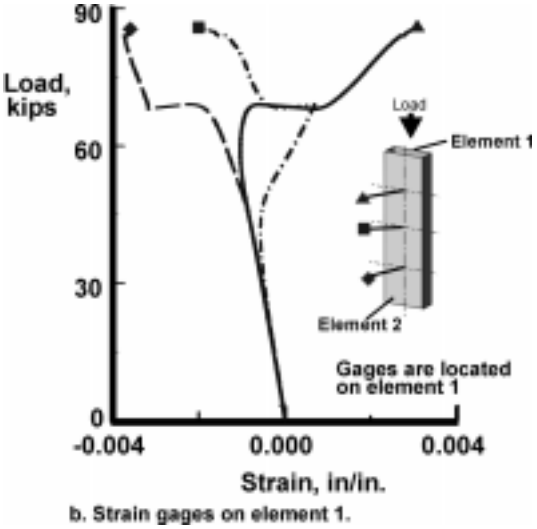

Figure 21. - Strain gage results along centerline of NEF specimen with b/t = 45.

The ratio of the crippling strength to the laminate ultimate strength for the NEF carbon-rod reinforced specimens are compared in figure 23 with the MIL-HDBK-17E (reference 10) recommended preliminary design curves (figure 4.7.2(f)) for the [$\pm$45/0$_n$/$\pm$45] carbon-tape laminates. The strength ratios for the NEF specimens (figure 23) compare well with the predicted strength failure ratios from the preliminary design curves. These results suggest that using the carbon-tape preliminary design curves for the design of carbon-rod reinforced structure would give a very good approximation for the design of NEF elements.

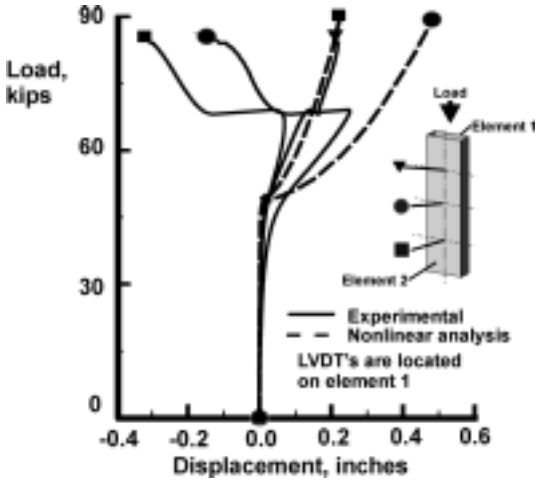

Figure 22. - Out-of-plane displacements on centerline of NEF specimen with b/t = 45.

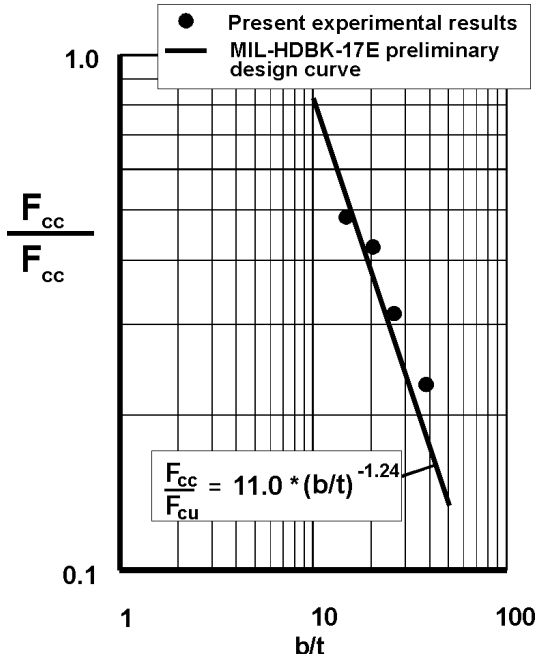

Figure 23. - Comparison of experimental results to MIL-HDBK-17 preliminary design curves.

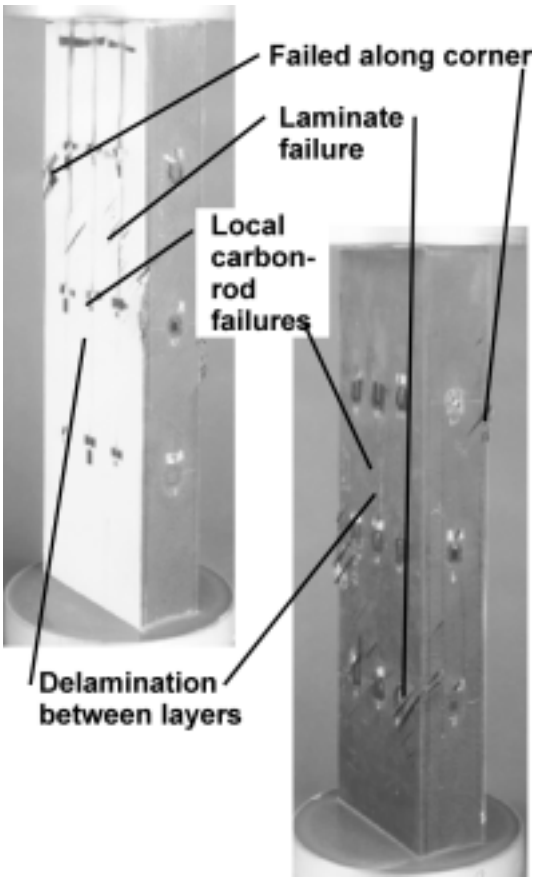

Figure 24. - Typical failure modes for NEF specimens.

Typical failure modes for the NEF specimens are shown in figure 24. All NEF specimens exhibited some failures in the corner radius location where the elements transitioned to the $\pm 45°$ tape laminate webs that support the elements. The NEF specimen with a b/t = 12.6 failed at the potted end of element 2 and approximately 4 inches from the potting on the end of element 1. The thickness of the elements of this specimen (b/t = 12.6) were thinner than the other specimens. The thickness varied from 0.205 in. adjacent to the failures, to a thickness of 0.213 in. at the opposite ends. The thickness of the other specimens varied from 0.220 in. to 0.222 in. for OEF and NEF specimens. Element 1 in the NEF specimen with a b/t = 19.4 failed at the specimen mid-length and element 2 delaminated at mid-length and the delamination extended to approximately the quarter points. Both elements of the NEF specimen with a b/t = 27 delaminated through the $\pm 45°$ plies between the rod layers from the mid-length point to the bottom end (as tested). The NEF specimen with b/t = 45 delaminated through the $\pm 45°$ plies between the carbon-rod layers at the bottom end (as tested) on both elements and extended for approximately 4 inches along the length of the specimen. A one-inch-wide delamination exists in element 1 through the $\pm 45°$ plies between the carbon-rod layers at approximately mid-length and extends 1 inch above and 4 inches below the mid-point.

The experimental results for the NEF specimens have been normalized by the more detailed non-dimensional crippling parameters presented in the previous section, and are shown in figure 25 for the NEF specimens. A curve is fitted through the data and the values of the curve fit parameters are shown in figure 25. These curves can be used to design the NEF carbon-rod reinforced structural elements. Test results of NEF specimens of graphite-thermoset and graphite-thermoplastic tape systems normalized to the same parameters are shown in MIL-HDBK-17E, figure 4.7.2.4(b) and are also shown in figure 25 for comparison. The tape data from MIL-HDBK-17E compare well the carbon-rod data for all b/t ratios.

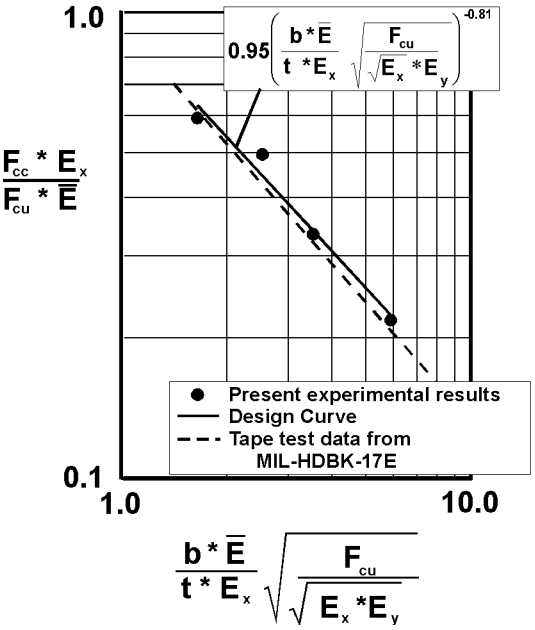

Figure 25. - Design curves for No-Edge-Free elements.

Summary

The experimental results of a study of the crippling strength of carbon-rod reinforced crippling elements has been used to develop empirical curves that can be used for the design of One-Edge-Free and No-Edge-Free carbon-rod reinforced crippling strength elements. The results also indicate that the use of carbon-tape preliminary design crippling strength curves to design carbon-rod crippling elements would result in a conservative design for the One-Edge-Free elements, and a very good approximation for the No-Edge-Free elements. It was shown that the STAGS finite element analysis accurately predicted the initial buckling loads and the geometric response after the initial buckling of the specimen.

References

1. Nunn, K. E. and Dompka, R. V., *DMLCC-BW PHASE I Interim Report for Period October 1991 - October 1992*, WL-TR-92-8009, November 1992.

2. Nunn, K. E. and Dompka, R. V., *DMLCC-BW Phase II Interim Report for Period October 1992 - October 1993*, WL-TR-94-8007, November 1994.

3. Baker, D. J., Nunn, K. E., Rogers, C. W., Dompka, R. V., and Holzwarth, R. C., *Design, Development and Test of a Low-Cost, Pultruded-Rod-Stiffened Wing Concept and its application to a Civil Tiltrotor Transport*, presented at the 10th DOD/NASA/FAA Conference on Fibrous Composites in Structural Design, November 1993, proceedings NAWCADWAR-94096-60, April 1994.

4. Rousseau, C. Q., Baker, D. J., and Chan, W. S., *Analysis and Testing of a Rod-Reinforced Hat-Section Stringer*, presented at the 36th Structures, Structural Dynamics and Materials Conference New Orleans, LA, April 10-12, 1995. AIAA Paper 95-1509.

5. Baker, D. J. and Rousseau, C. Q., *Design and Evaluation of a Bolted Joint for a Discrete Carbon-Epoxy Rod-Reinforced Hat Section*, presented at the 11th DOD/NASA/FAA Conference on Fibrous Composites in Structural Design, Ft. Worth, TX, August 1996, Proceedings WL-TR-97-3008, April 1997.

6. Rousseau, C. Q. and Baker, D. J., *Layer Termination in Rod-Reinforced Structures*, presented at the American Helicopter Society National Technical Specialists Meeting on Rotorcraft Structures, Williamsburg, VA, October 30 - November 2, 1995

7. Baker, D. J. and Rogers, C., *Analysis and Tests of Reinforced Carbon-Epoxy/Foam—Core Sandwich Panels With Cutouts*, presented at the American Helicopter Society 52nd Annual Forum, Washington, D.C. June 4-6, 1996 and published the American Helicopter Society Journal, Vol. 43, No. 2, April 1998, pp 120-132

8. Anderson, T. C., Holtzwarth, R. C., *Design and Manufacture of Low-Cost Composite-Bonded Wing*, presented at the 39th Structures, Structural Dynamics and Materials Conference Long Beach, Ca, April 20-23, 1998, AIAA Paper 98-1870.

9. Cronkhite, J. D., Dompka, R., Anderson, T., *Cost and Performance of a Bonded IML-Tooled Tiltrotor Wing*, presented at the American Helicopter Society National Specialists Meeting on Affordable Composite Structures, Bridgeport, CO, October 7 and 8, 1998.

10. Anonymous, MIL-HDBK-17E, Volume 3, January 23, 1997.

11. Brogan, F. A., Rankin, C. C., and Cabiness, H. D., *STAGS Users Manual*, Lockheed Palo Alto Research Laboratory, Report LMSC P032594, 1994.